final ΔF map had a background of ± 0.5 e/Å^3.

The scattering curves were taken from Cromer and Waber[17] except for that of hydrogen, which was from Stewart et al.[18]

NMR and ESR Spectra. Proton spectra were measured on a Varian XL-200 FT spectrometer. The inept spectrum shown in Figure 3 was measured on a Varian XL-300 FT machine at 59.59 MHz. The sample was a saturated solution in THF at -80 °C and was referenced to external Me_4Si in $CDCl_3$ (1:1 (v/v)) at ambient temperature. The following pulse sequence was used for the proton-decoupled spectrum: 90°(H, x)-$\tau/2$-180°(H, x), 180°(Si, x)-$\tau/2$-90°(H, y), 90°(Si, x)-$\Delta/2$-180°(H, x), 180°(Si, x)-$\Delta/2$-decouple-acquire.

For both coupled and decoupled spectra the following parameters were used: $PW(90°)_H$ = 41.1 μ_s, $PW(90°)_{Si}$ = 21.5 μ_s. The FIDs were collected into 32 K data points. Since no silicon satellites were observed in the ^1H spectrum, a J value of 200 Hz was initially used, based on the reported value for $PhSiH_3$.[19] A spectral width of 50 KHz was employed with a digital resolution of 3.3 Hz. A refocussing delay of 1.67 ms was used in conjunction with an excitation delay of 2.5 ms and an equilibrium delay of 2 s. A coupled spectrum was subsequently run with use of the same conditions to obtain a more accurate J_{Si-H} value, and the parameters were then modified to optimize the coupled spectrum. The modified parameters were J_{Si-H} = 150 Hz, spectral width = 7142.9 Hz, digital resolution = 0.45 Hz, excitation transfer delay = 3.33 ms, and equilibrium delay = 1 s.

Acknowledgment. This work was supported by grants from the Natural Sciences and Engineering Research Council of Canada, the Fonds FCAC de Québec, and the Dow Corning Corp. Two of us (J.F.H. and E.S.) thank the Governments of France and Québec for travel grants in support of this project. Valuable discussions with Dr. D. Gourier, Laboratoire de la chimie de la matière condensée, ENSCP, on the subject of ESR spectra, and with Dr. M. Simard, Laboratoire des structures aux rayons-X, concerning the crystal structures, are gratefully acknowledged.

Supplementary Material Available: Calculated positions for hydrogen atoms of phenyl groups and Cp rings for **2** (Table VII) and **3** (Table VIII), anisotropic thermal parameters for non-hydrogen atoms of **2** (Table IX) and **3** (Table X), and calculated and observed structure factor amplitudes for **2** (Table XI) and **3** (Table XII) (6 pages). Ordering information is given on any current masthead page.

(17) Cromer, D. T.; Waber, J. T. *Acta Crystallogr.* **1965**, *18*, 104.
(18) Stewart, R. F.; Davidson, E. R.; Simpson, W. T. *J. Chem. Phys.* **1965**, *42*, 3175.
(19) Jensen, M. A. *J. Organomet. Chem.* **1968**, *11*, 423.

Hydride Transfer in the Oxidation of Formate Ion by $[(bpy)_2(py)Ru(O)]^{2+}$

Lee Roecker and Thomas J. Meyer*

Contribution from the Department of Chemistry, The University of North Carolina, Chapel Hill, North Carolina 27514. *Received October 1, 1985*

Abstract: The kinetics of oxidation of formic acid/formate ion by $[(bpy)_2(py)Ru^{IV}(O)]^{2+}$ (bpy is 2,2′-bipyridine and py is pyridine) have been studied as a function of pH and temperature, and the kinetics of oxidation of HCO_2^- by $[(bpy)_2(py)Ru^{III}(OH)]^{2+}$ have been studied at pH 7. The pH dependence of the Ru^{IV} reaction is consistent with paths involving oxidation of HCO_2H, k (25 °C, μ = 0.1 M) = 0.01 ± 0.04 M^{-1} s^{-1}, and of HCO_2^-, k (25 °C, μ = 0.1 M) = 4.2 ± 0.2 M^{-1} s^{-1}. For the oxidation of HCO_2^- by Ru^{III}, k (25 °C, μ = 1.0 M, pH 7) = 0.01 M^{-1} s^{-1}. The path involving Ru^{IV} and HCO_2^- exhibits a large kinetic isotope effect with $k_{HCO_2^-}/k_{DCO_2^-}$ = 19 (25 °C, μ = 1.0 M) while that involving Ru^{III} and HCO_2^- has a much smaller kinetic isotope effect with $k_{HCO_2^-}/k_{DCO_2^-}$ = 3 (25 °C, μ = 1.0 M). Spectral evidence, in conjunction with the isotope effect data, suggests that oxidation of HCO_2^- by $[(bpy)_2(py)Ru^{IV}(O)]^{2+}$ occurs by a two-electron, hydride transfer which is discussed in some detail. Oxidation of HCO_2^- by $[(bpy)_2(py)Ru^{III}(OH)]^{2+}$ appears to occur by outer-sphere electron transfer.

An important theme in our recent work has been the preparation and characterization of polypyridyl oxo complexes of ruthenium(IV)[1,2] and an examination of their abilities as stoichiometric and catalytic oxidants.[3,4] The results of mechanistic studies suggest that oxidation of 2-propanol to acetone[5] and of cumene to cumyl alcohol[6] proceed by two-electron, hydride transfers, e.g., reaction 1′, oxidation of hydrogen peroxide to oxygen via hydrogen atom transfer,[7] and oxidation of PPh_3 to $OPPh_3$ by O-atom transfer.[8] One of the notable features about the polypyridyl complexes as oxidants is that they are easily amenable to kinetic studies and detailed mechanistic investigations based on ^{18}O labeling, pH dependence, H/D kinetic isotope effects, and initial product studies the latter of which can sometimes allow a distinction to be drawn between one- and two-electron pathways.

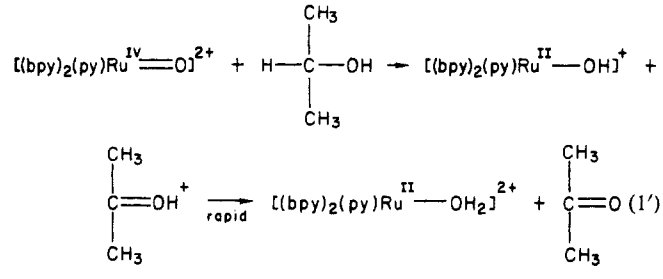

We report here a detailed study on the oxidation of formate ion and formic acid by $[(bpy)_2(py)Ru(O)]^{2+}$ to give CO_2. In addition to a general interest in C-based redox chemistry, two points drew our attention to the formate/formic acid reaction. The first is that the oxidation of formate by a variety of oxidants has been reported which allows for comparisons to be made between their reactivity characteristics and those of oxo complexes

(1) (a) Moyer, B. A.; Meyer, T. J. *Inorg. Chem.* **1981**, *20*, 436. (b) Dobson, J., work in progress.
(2) Takeuchi, K. J.; Thompson, M. S.; Pipes, D. W.; Meyer, T. J. *Inorg. Chem.* **1984**, *23*, 1845.
(3) (a) Thompson, M. S.; DeGiovani, W. F.; Moyer, B. A.; Meyer, T. J. *J. Org. Chem.* **1984**, *49*, 4972. (b) Moyer, B. A.; Thompson, M. S.; Meyer, T. J. *J. Am. Chem. Soc.* **1980**, *102*, 2310.
(4) Meyer, T. J. *J. Electrochem. Soc.* **1984**, *131*, 221C.
(5) (a) Thompson, M. S.; Meyer, T. J. *J. Am. Chem. Soc.* **1982**, *104*, 4106. (b) Roecker, L.; Meyer, T. J., submitted for publication.
(6) Thompson, M. S.; Meyer, T. J. *J. Am. Chem. Soc.* **1982**, *104*, 5070.
(7) (a) Gilbert, J. A.; Gersten, S. W.; Meyer, T. J. *J. Am. Chem. Soc.* **1982**, *104*, 6872. (b) Gilbert, J. A.; Roecker, L.; Meyer, T. J., manuscript in preparation.
(8) Moyer, B. A.; Sipe, B. K.; Meyer, T. J. *Inorg. Chem.* **1981**, *20*, 1475.

0002-7863/86/1508-4066$01.50/0

of Ru^{IV}. The second was the possibility of gaining insight into possible pathways for the more interesting microscopic reverse reaction, the reduction of CO_2 to formate.

Experimental Section

Materials. House distilled water was purified by distillation from alkaline permanganate. Sodium formate from the Aldrich Chemical Company was recrystallized twice from water and dried in a vacuum oven. DCO_2D, 99.8 atom %, obtained from the Stohler Chemical Company, Waltham, MA and D_2O, 99.8 atom %, from Aldrich, were used without further purification. All other materials were reagent grade and used without further purification.

Preparations. The salts $[Ru(bpy)_2(py)(OH_2)](ClO_4)_2$ and $[Ru(bpy)_2(py)(O)](ClO_4)_2$ were prepared by previously reported procedures.[1a]

Instrumentation. Routine UV–vis spectra were recorded on Bausch and Lomb Spectronic 2000 or Hewlett Packard 8450A Diode Array spectrophotometers. pH was measured by using a Radiometer pHM62 pH meter. Coulometric measurements were performed at room temperature by using a PAR Model 173 Potentiostat/Galvanostat. Reticulated vitreous carbon electrodes, 12 holes for 1 linear in. (ERG, Inc., Oakland, CA), were used in the coulometric determinations. Gas chromatographic measurements were performed on a Hewlett Packard 5890A Gas Chromatograph equipped with a Porapak Q column (Alltech Associates, Inc., Deerfield, IL) using He as the carrier gas. Stopped-flow measurements were carried out on an Aminco-Morrow stopped-flow apparatus attached to a Beckman DU monochrometer, details of which are given elsewhere.[9] Calculations were performed on a Commodore PET Computer Model 4032 using locally written programs or for curve fitting the UNC VAX-11 system using RS/1 software by BBN Research Systems. The program uses a nonlinear least-squares analysis.

Kinetic Measurements on $[(bpy)_2(py)Ru(O)](ClO_4)_2$ as Oxidant. Rate data for the disappearance of Ru^{IV} were collected by following the absorbance increase at 397 nm. This wavelength is an isosbestic point for $[(bpy)_2(py)Ru^{III}(OH)]^{2+}$ and $[(bpy)_2(py)Ru^{II}(OH_2)]^{2+}$ and as such, at this wavelength the disappearance of Ru^{IV} can be followed without interference from the subsequent reduction of Ru^{III} to Ru^{II}. Plots of $\ln |A_\infty - A_t|$ vs. time were linear, and first-order rate constants were calculated on the basis of a least-squares fit (uniform weighting) to the relation

$$\ln |A_\infty - A_t| = -kt + \ln |A_\infty - A_0|$$

where A_∞ is the final absorbance at completion of the reaction, A_0 is the initial absorbance, A_t is the absorbance measured at time t, and k is the first-order rate constant. A_∞ readings were obtained for each run, and data from the first 4 half-lives were used in determining k. The observed rate constants were invariant to changes in concentration of either oxidant over the range 10^{-4}–5×10^{-4} M. Ionic strengths were varied from 0.10 M to 1.00 M with Na_2SO_4. In some experiments $NaClO_4$ was used to maintain ionic strength. Small differences were observed between the two electrolytes. pH was controlled with phosphate buffers, and reaction rates were independent of the buffer concentration. Purging reaction solutions with Ar prior to use had no apparent effect on the kinetics so no attempts were made to achieve anaerobic conditions. Formate concentrations were determined by titration of formic acid solutions prior to dilution with buffer solutions or by weighing $NaCO_2H$ and dissolving the solid in buffer. Rate constants obtained from the two procedures agreed to within 5%.

Kinetic Measurement Based on $[(bpy)_2(py)Ru(OH)]^{2+}$ as Oxidant. Two approaches were used in studying the reactivity of the Ru^{III} complex with formate. Method A: in one approach, rate data were collected by mixing Ru^{IV} with formate and monitoring the subsequent spectral increase at 470 nm instead of 397 nm. Plots of $\ln |A_\infty - A_t|$ vs. time for the 470-nm data were nonlinear. At 470 nm the initial curved portion of the plot arises from the reaction of Ru^{IV} while the later, linear portion of the plot monitors the reduction of Ru^{III} to Ru^{II}. The slope of the limiting, linear portion was taken as the rate constant for the reaction of Ru^{III} with formate.[10] Method B: as a check, a second approach was undertaken where $[(bpy)_2(py)Ru(OH)]^{2+}$ was generated in situ by mixing $[(bpy)_2(py)Ru(O)]^{2+}$ with an excess of $[(bpy)_2(py)Ru(H_2O)]^{2+}$.[11] The resulting solution was mixed with formate, and spectral changes were monitored at 470 nm. Plots of $\ln |A_\infty - A_t|$ vs. time were linear, and the rate constants which resulted from the treatment were within 8% of those obtained in the first approach.

(9) Cramer, J. L. Ph.D. Dissertation, The University of North Carolina, Chapel Hill, NC, 1975, pp 191–216.
(10) For more details of this treatment see ref 5.
(11) Binstead, R. A.; Moyer, B. A.; Samuels, G. J.; Meyer, T. J. *J. Am. Chem. Soc.* **1981**, *103*, 2897.

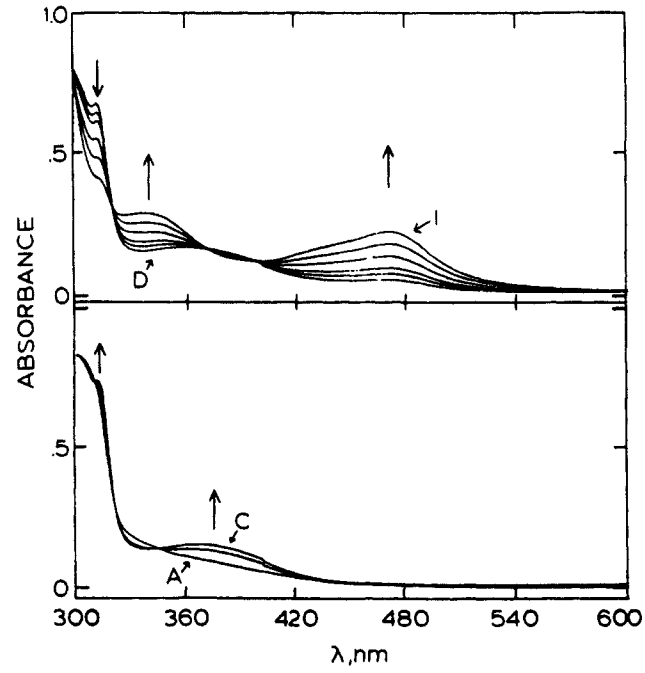

Figure 1. Successive spectral scans during the oxidation of formate by $[(bpy)_2(py)Ru(O)]^{2+}$ in pH 7.0 phosphate buffer after (A) 0, (B) 10, (C) 20, (D) 90, (E) 140, (F) 190, (G) 360, (H) 900, and (I) 2700 s.

Results

Stoichiometry. The overall stoichiometry of the oxidation is 1:1, as determined by a spectrophotometric titration of $[(bpy)_2(py)Ru(O)]^{2+}$ with formate in unbuffered water and monitoring at 470 nm which is a λ_{max} for the aqua product.

$$H^+ + [(bpy)_2(py)Ru(O)]^{2+} + HCO_2^- \rightarrow [(bpy)_2(py)Ru(H_2O)]^{2+} + CO_2$$

Product Analysis. CO_2 generated by the electrocatalytic oxidation of HCO_2^- was shown to be the oxidation product via gas chromatography. In one experiment 0.0035 g of $[(bpy)_2(py)Ru(H_2O)](ClO_4)_2$ were dissolved in 20 mL of 0.103 M sodium formate and electrolyzed at 0.8 V by using a reticulated vitreous carbon electrode in a three-arm electrolysis cell. In the experiment, $[(bpy)_2(py)Ru(O)]^{2+}$ generated electrochemically is reduced to $[(bpy)_2(py)Ru(H_2O)]^{2+}$ by formate and then regenerated at the electrode which allows for large amounts of CO_2 to be built up in the cell. After 6.7×10^{-5} equiv had been passed, the electrolysis was stopped, and the solution was acidified. GC analysis of the air space above the acidified solution clearly indicated the presence of significant amounts of CO_2 although no attempt was made to quantify the amount of CO_2 produced. The ruthenium product after the reaction of $[(bpy)_2(py)Ru(O)]^{2+}$ with formate is $[(bpy)_2(py)Ru(H_2O)]^{2+}$ as shown by cyclic voltammetry and UV–vis spectroscopy.

Kinetics. Figure 1 shows the spectral changes accompanying the oxidation of formate by $[(bpy)_2(py)Ru(O)]^{2+}$. Two stages are evident, the faster process being attributable to the oxidation by $[(bpy)_2(py)Ru^{IV}(O)]^{2+}$ and the slower to the oxidation by $[(bpy)_2(py)Ru^{III}(OH)]^{2+}$. Kinetics of the faster process were monitored at 397 nm, and the data collected are given in Table I. The reaction is first order in formate over the concentration range cited in Table I. At pH 7 the experimental rate law can be described by

$$-d[Ru^{IV}]/dt = k[HCO_2^-]_T[Ru^{IV}] = k_{obsd}[Ru^{IV}] \quad (1)$$

where $[HCO_2^-]_T$ is total formate ion plus formic acid, $k = 4.2 \pm 0.2$ M^{-1} s^{-1} at 25 °C, $\mu = 0.10$ M ($NaClO_4$), and $k = 4.5 \pm 0.2$ M^{-1} s^{-1} at 25.6 °C, $\mu = 1.0$ M (Na_2SO_4). Decreasing the ionic strength to 0.10 M (Na_2SO_4) resulted in an increase in k to 6.7 M^{-1} s^{-1} as expected for a reaction involving reactants of opposite charge types.

Table I. Observed Pseudo-First-Order Rate Constants and Calculated Second-Order Rate Constants for the Oxidation of Formate/Formic Acid by $[(bpy)_2(py)Ru(O)]^{2+}$ and $[(bpy)_2(py)Ru(OH)]^{2+}$

pH	$[formate]_T$	$10^3 \times k_{obsd}$ (s^{-1})[a]	k (M^{-1} s^{-1})
		$[(bpy)_2(py)Ru(O)]^{2+}$	
7.00	0.1290	557	4.32
7.00	0.0800	335	4.19
7.00	0.0400	170	4.25
7.00	0.0080	34.7	4.33
8.12	0.0800	335	4.18
6.56	0.0800	332	4.15
5.71	0.0800	326	4.08
5.24	0.0800	330	4.13
4.28	0.0800	288	3.60
3.88	0.0800	242	3.03
3.68	0.0800	157	1.96
3.22	0.0800	100	1.25
2.78	0.0800	44.2	0.552
1.91	0.0800	12.3	0.154
1.56	0.0800	4.89	0.0611
1.32	0.0800	3.38	0.0423
1.07	0.0800	1.87	0.0234
1.00	0.0423	0.669	0.0158
1.00	0.0282	0.418	0.0148
1.00	0.0564	0.811	0.0144
1.00	0.0056	0.086	0.0152
		$[(bpy)_2(py)Ru(OH)]^{2+}$ [b]	
7.00	0.0423	0.460[c]	0.011
7.00	0.0423	0.600[d]	0.014

[a] Average of five determinations from pH 8.12 to pH 3.22, from pH 2.78 to pH 1.00 k_{obsd} is from a single determination. μ = 0.10 M ($NaClO_4$), 25.5 ± 0.1 °C. Values of k_{obsd} are ±5%. $k = k_{obsd}/[HCO_2^-]_T$ where $[HCO_2^-]_T$ = [formate]$_T$ is total formate. [b] μ = 1.0 M (Na_2SO_4). [c] Method A (note Experimental Section)—2 determinations. [d] Method B (note Experimental Section)—2 determinations.

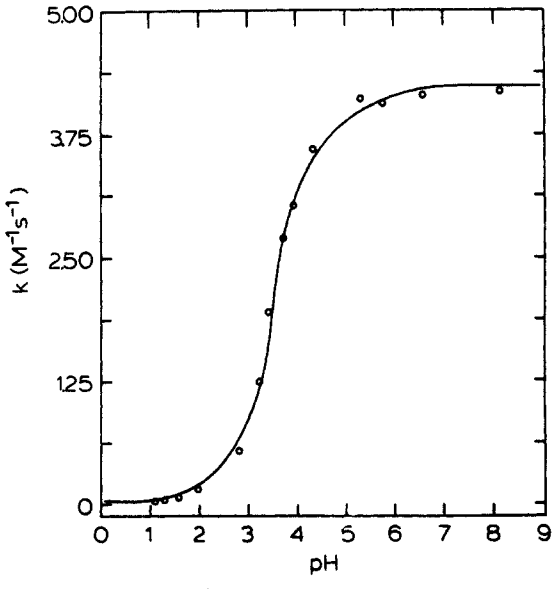

Figure 2. Plot of k (M^{-1} s^{-1}) vs. pH for the oxidation of formate/formic acid by $[(bpy)_2(py)Ru(O)]^{2+}$ at 25 °C, μ = 0.10 M ($NaClO_4$).

Values of $k = k_{obsd}/[HCO_2^-]_T$ are pH dependent in more acidic solutions as illustrated in Figure 2, where k ranges from 0.015 M^{-1} s^{-1} at pH 1 to 4.2 M^{-1} s^{-1} at pH 7. The pH dependence is in accord with the reaction scheme

$$HCOOH \rightleftharpoons HCO_2^- + H^+ \qquad K_a$$

$$[(bpy)_2(py)Ru(O)]^{2+} + HCOOH \rightarrow \text{products} \qquad k_1$$

$$[(bpy)_2(py)Ru(O)]^{2+} + HCO_2^- \rightarrow \text{products} \qquad k_2$$

which leads to[12]

$$k = \frac{k_1[H^+] + k_2K_a}{[H^+] + K_a} \qquad (2)$$

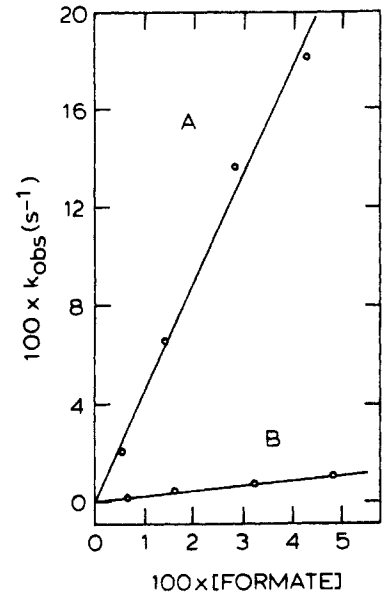

Figure 3. Plot of k_{obsd} vs. (A) $[HCO_2^-]$ and (B) $[DCO_2^-]$ at 25.6 °C, pH 7 phosphate buffer, μ = 1.00 M (Na_2SO_4) for oxidation by $[(bpy)_2(py)Ru(O)]^{2+}$.

Best fit values for k_1, k_2, and K_a were calculated based on the experimental values for k as a function of $[H^+]$ and the equation above as described in the Experimental Section. The best fit values were k_1 = 0.01 ± 0.04, k_2 = 4.2 ± 0.2, and K_a = (2.4 ± 0.2) × 10^{-4}. The curve in Figure 2 is drawn by using these parameters in eq 2. The calculated value of K_a is in reasonable agreement with that reported for the K_a of formic acid (1.78 × 10^{-4}). Linearization of eq 2[12] and use of K_a = 1.78 × 10^{-4} yielded a straight line (r = 0.997) and values of k_1 and k_2 within experimental error of those obtained by the nonlinear fitting procedure. The relative slowness of the k_1 path results in a large numerical uncertainty for its magnitude, and, statistically, there is no guarantee that such a path plays a significant role. The error associated with the k_1 term is large and might improve if more data in the range from pH 0 to 1 were available. Solubility problems prevented further data acquisition in the perchlorate medium, and the point was not pursued further.

Also given in Table I are the observed rate constants for the oxidation of formate by $[(bpy)_2(py)Ru^{III}(OH)]^{2+}$. The oxidation by Ru^{III} proceeds ca. 350 times slower than oxidation by $[(bpy)_2(py)Ru^{IV}(O)]^{2+}$ and accounts for the slower process shown in Figure 1.

Results are given in Table II for solvent and substrate kinetic isotope effects. A relatively insignificant inverse solvent kinetic isotope effect (k_{H_2O}/k_{D_2O}) was found for the reaction between $[(bpy)_2(py)Ru(O)]^{2+}$ and HCO_2^-. A large deuterium isotope effect is observed for the oxidation of HCO_2^- by $[(bpy)_2(py)Ru(O)]^{2+}$ with $k(HCO_2^-)/k(DCO_2^-)$ = 19 ± 3 (Figure 3). A much smaller isotope effect exists for the oxidation of formate by $[(bpy)_2(py)Ru(OH)]^{2+}$ with $k(HCO_2^-)/k(DCO_2^-)$ = 3–4.

Activation Parameters. Activation parameters for the reactions between $[(bpy)_2(py)Ru(O)]^{2+}$ and HCO_2^- or DCO_2^- were obtained from plots of ln (k/T) vs. $1/T$ at pH 7 (Figure 4) or ln k vs. $1/T$ over the temperature range 16–38 °C (Supplementary Table A). The results obtained were as follows: for HCO_2^-, $\Delta H^\ddagger$ = 7.7 ± 0.5 kcal/mol (E_a = 7.9 ± 0.9 kcal/mol) and $\Delta S^\ddagger$ = −30 ± 2 eu [A = (2.6 ± 1.0) × 10^6 s^{-1}]; for DCO_2^-, $\Delta H^\ddagger$ = 10.8 ± 0.7 kcal/mol (E_a = 11.1 ± 0.9 kcal/mol) and $\Delta S^\ddagger$ = −25 ± 2 eu [A = (1.7 ± 1.0) × 10^7 s^{-1}]. Activation parameters were not determined for the oxidation of formate by $[(bpy)_2(py)Ru(OH)]^{2+}$.

One- vs. Two-Electron Transfer. The magnitude of the H/D isotope effect for formate ion oxidation points to an important role for the H–CO_2^- bond in the redox step. The question remains

(12) Wilkins, R. G. *The Study of Kinetics and Mechanism of Reactions of Transition Metal Complexes*, Allyn and Bacon: Boston, 1974; pp 43–46.

Table II. Kinetic Isotope Effects for the Oxidation of Formate by $[(bpy)_2(py)Ru(O)]^{2+}$ at 25.5 ± 0.1 °C, pH 7, μ = 1.0 M (Na_2SO_4)

oxidant	k_{H_2O}	k_{D_2O}	k_{H_2O}/k_{D_2O}	$k_{HCO_2^-}$	$k_{DCO_2^-}$	$k_{HCO_2^-}/k_{DCO_2^-}$
$[(bpy)(py)Ru(O)]^{2+}$	4.5	4.7[a]	0.96	4.5 ± 0.2	0.24 ± 0.01	19 ± 3
$[(bpy)(bpy)Ru(OH)]^{2+}$				0.011[b]	0.038[b]	3
				0.014[c]	0.0034[c]	4

[a] Average of five determinations at a single concentration. [b] Method A; see Experimental Section. [c] Method B; see Experimental Section.

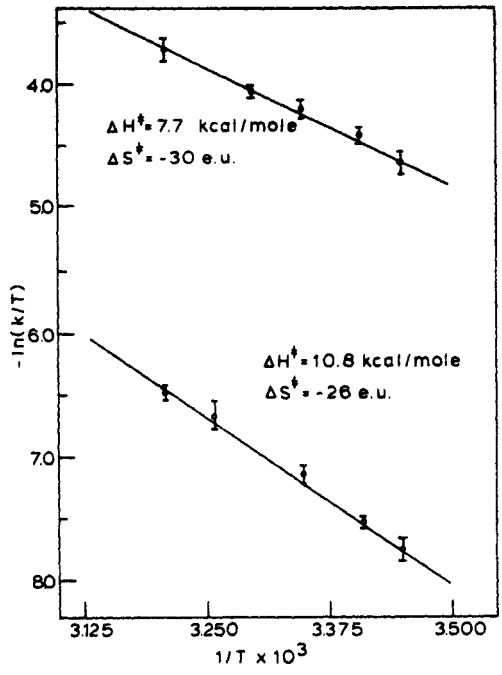

Figure 4. Plots of ln k/T vs. $1/T$ for the oxidation of HCO_2^- (top) and DCO_2^- (bottom) by $[(bpy)_2(py)Ru(O)]^{2+}$ at pH 7, μ = 1.00 M (Na_2SO_4).

however as to whether the redox step involves a net two-electron transfer and the direct production of CO_2

$$(bpy)_2(py)Ru^{IV}{=}O^{2+} + H{-}CO_2^- \rightarrow (bpy)_2(py)Ru^{II}{-}OH^+ + CO_2 \quad (3)$$

or an initial one-electron step

$$(bpy)_2(py)Ru^{IV}{=}O^{2+} + H{-}CO_2^- \rightarrow (bpy)_2(py)Ru^{III}{-}OH^{2+} + CO_2^- \quad (4)$$

followed by oxidation of CO_2^- by $Ru^{IV}{=}O^{2+}$, $Ru^{III}{-}OH^{2+}$, or O_2.

Mechanisms for the two possibilities are illustrated in Scheme I.

Scheme I

Mechanism A ($1e^-/1H^+$—"H-atom" transfer)

$$(bpy)_2(py)Ru^{IV}{=}O^{2+} + HCO_2^- \rightarrow (bpy)_2(py)Ru^{III}{-}OH^{2+} + CO_2^-$$

$$(bpy)_2(py)Ru^{III}{-}OH^{2+} + H^+ + CO_2^- \xrightarrow[fast]{} (bpy)_2(py)Ru^{II}{-}OH_2^{2+} + CO_2$$

$$\{(bpy)_2(py)Ru^{IV}{=}O^{2+} + CO_2^- + H^+ \xrightarrow[fast]{fast} (bpy)_2(py)Ru^{III}{-}OH^{2+} + CO_2\}$$

Mechanism B ($2e^-/1H^+$—"hydride" transfer)

$$(bpy)_2(py)Ru^{IV}{=}O^{2+} + HCO_2^- \rightarrow (bpy)_2(py)Ru^{II}{-}OH^+ + CO_2$$

$$(bpy)_2(py)Ru^{II}{-}OH^+ + H^+ \xrightarrow[fast]{} (bpy)_2(py)Ru^{II}{-}OH_2^{2+}$$

Comproportionation

$$(bpy)_2(py)Ru^{IV}{=}O^{2+} + (bpy)_2(py)Ru^{II}{-}OH_2^{2+} \rightarrow 2(bpy)_2(py)Ru^{III}{-}OH^{2+}$$

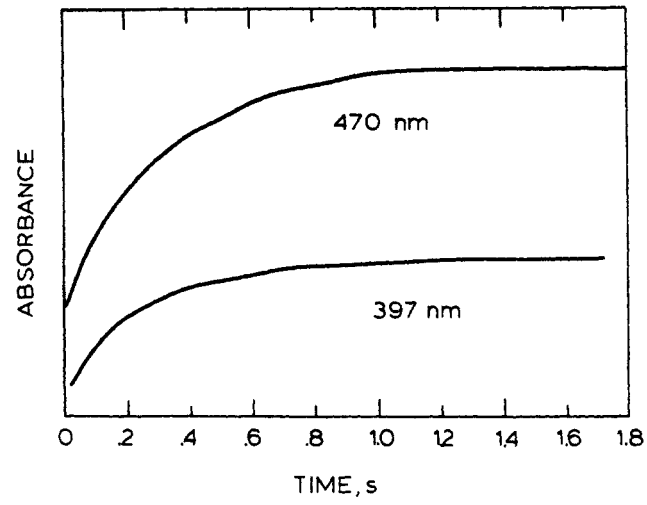

Figure 5. Absorbance traces obtained by stopped-flow monitoring of the oxidation of HCO_2^- by $[(bpy)_2(py)Ru(O)]^{2+}$ with $[HCO_2^-]$ = 3.5 M at 397 nm and 470 nm in D_2O.

The fundamental difference between the two is that the rate-determining redox step in mechanism A involves a $1e^-/1H^+$ or H-atom transfer from reductant to Ru^{IV}–oxo while in mechanism B, a $2e^-/1H^+$ or hydride transfer is involved.

In principle, a distinction between the $1e^-$ and $2e^-$ steps can be made depending on whether $[(bpy)_2(py)Ru^{II}(OH_2)]^{2+}$ or $[(bpy)_2(py)Ru^{III}(OH)]^{2+}$ is the initial product since their absorption spectra differ significantly.[1a] However, there is a complication since $[(bpy)_2(py)Ru^{II}(OH_2)]^{2+}$ once formed undergoes rapid comproportionation (Scheme I) (k (25 °C, μ = 0.1 M) = 2×10^5 M^{-1} s^{-1}) with $[(bpy)_2(py)Ru^{IV}(O)]^{2+}$ to give $2[(bpy)_2(py)Ru^{III}(OH)]^{2+}$.[11]

At the relatively low formate concentration used to generate Figure 1, the initial oxidation rate is slow compared to comproportionation, and $[(bpy)_2(py)Ru^{III}(OH)]^{2+}$ would be the initial product regardless of whether $1e^-$ or $2e^-$ mechanisms are operative. However, a distinction between the two can be made based on Ru^{II} or Ru^{III} as initial product by using stopped-flow monitoring at sufficiently high formate levels that $k_{IV}[HCO_2^-][Ru^{IV}] > k_{com}[Ru^{IV}][Ru^{II}]$. Rapid monitoring is required because the following, slower oxidation of HCO_2^- by $[(bpy)_2(py)Ru^{III}(OH)]^{2+}$ also gives $[(bpy)_2(py)Ru^{II}(OH_2)]^{2+}$.

As shown in Figure 5, in D_2O at $[HCO_2^-]$ = 3.5 M, the rate of disappearance of $[(bpy)_2(py)Ru^{IV}(O)]^{2+}$ monitored at the Ru^{III}/Ru^{II} isosbestic point at 397 nm is equal to the rate of appearance of $[(bpy)_2(py)Ru(OH_2)]^{2+}$ at 470 nm. Within the limits of accuracy of the experiment Ru^{II} *must* be the initial product. The key to the experiment is the use of D_2O as solvent since the rate of formate oxidation is relatively unaffected in D_2O compared to H_2O, but the rate constant for comproportionation is decreased by a factor of 16 in D_2O.[11]

The same conclusion was reached by using neat methanol as solvent. Addition of solid $[(bpy)_2(py)Ru(O)]^{2+}$ to methanol which had been saturated with sodium formate instantly yielded an orange solution whose spectral characteristics were indistinguishable from those of an authentic sample of $[(bpy)_2(py)Ru(OH_2)]^{2+}$ in the same solvent.[13]

(13) There is a reaction between $[(bpy)_2(py)Ru(O)]^{2+}$ and methanol, but it is much slower, $t_{1/2}$ ~50 s.

Scheme II[a]

mechanism	$\Delta G°'$, kcal/mol
1e⁻ hydrogen atom pathways	
1.1 $Ru^{II}{=}O^{2+} + HCO_2H \rightarrow Ru^{III}{-}OH^{2+} + HCO_2$	−12.2
1.2 $Ru^{IV}{=}O^{2+} + HCO_2^- \rightarrow Ru^{III}{-}OH^{2+} + CO_2^-$	−15.2
1.3 $Ru^{IV}{=}O^{2+} + HCO_2^- \rightarrow Ru^{III}{-}O^+ + H + CO_2$[b]	≥28.4
1e⁻ outer-sphere pathway	
1.4 $Ru^{IV}{=}O^{2+} + HCO_2^- \rightarrow Ru^{III}{-}O^+ + HCO_2$[b]	≥−0.05
2e⁻ hydride pathways	
1.5 $Ru^{IV}{=}O^{2+} + HCO_2H \rightarrow Ru^{II}{-}OH^+ + CO_2 + H^+$	−31.6 (pH = 2)
1.6 $Ru^{IV}{=}O^{2+} + HCO_2^- \rightarrow Ru^{II}{-}OH^+ + CO_2$	−43.1
1.7 $Ru^{IV}{=}O^{2+} + HCO_2H \rightarrow Ru^{II}{-}OH_2^{2+} + CO_2$	−60.9
1.8 $Ru^{IV}{=}O^{2+} + HCO_2^- \rightarrow Ru^{IV}{=}O^{2+} + H^- + CO_2$[c]	+92.0

[a] Calculations based on the data in Figure 6. $Ru^{IV}{=}O^{2+}$ = $[(bpy)_2(py)Ru(O)]^{2+}$, $Ru^{III}{-}OH^{2+}$ = $[(bpy)_2(py)Ru(OH)]^{2+}$, and $Ru^{II}{-}OH_2^{2+}$ = $[(bpy)_2(py)Ru(OH_2)]^{2+}$. [b] Using $pK_a > 13$ for $[(bpy)_2(py)Ru^{III}(OH)]^{2+}$. [c] Calculated using $E° = -2.25$ V (vs. NHE) for the H^+/H^- couple (Latimer, W. M. *Oxidation Potentials*; Prentice-Hall: Englewood Cliffs, NJ, 1952).

Discussion

Rate Laws. The pH dependence of k_{obsd} for the oxidation of formate by $[(bpy)_2(py)Ru(O)]^{2+}$ is consistent with the rate law given in eq 5

$$-d[Ru^{IV}]/dt = k_1[HCO_2H][Ru^{IV}] + k_2[HCO_2^-][Ru^{IV}] \quad (5)$$

where $k_1 = 0.01 \pm 0.04$ M^{-1} s^{-1} and $k_2 = 4.2 \pm 0.2$ M^{-1} s^{-1} (25 °C, μ = 0.1 M, $NaClO_4$). Activation parameters and isotope effects were determined at pH 7.0 for only the k_2 term. For comparative purposes we also investigated the kinetics of oxidation of formate by $[(bpy)_2(py)Ru(OH)]^{2+}$ at pH 7. This is a somewhat difficult experiment because in competition with the direct reaction between $Ru^{III}{-}OH^{2+}$ and HCO_2^- is a pathway involving initial disproportionation, $2Ru^{III}{-}OH^{2+} \rightarrow Ru^{IV}{=}O^{2+} + Ru^{II}{-}OH_2^{2+}$, followed by oxidation of HCO_2^- by $Ru^{IV}{=}O^{2+}$.[5a] As outlined in the Experimental Section two methods were used to study this reaction. Agreement between the two methods was fair at best, and our inability to acquire kinetically precise rate constant data limited our studies to the determination of the rate constant and H/D kinetic isotope effect at pH 7.

Mechanistic Considerations. In addition to the rate law, a number of additional results bear directly on the question of mechanism. Most striking is the observation of a significant $k_{HCO_2^-}/k_{DCO_2^-}$ kinetic isotope effect of 19 ± 3 in the oxidation of formate by $[(bpy)_2(py)Ru(O)]^{2+}$. Large kinetic isotope effects have also been reported involving $[(bpy)_2(py)Ru(O)]^{2+}$ and 2-propanol,[5] hydrogen peroxide,[7] and $[(bpy)_2(py)Ru(OH_2)]^{2+}$.[11]

From the combination of rate law, kinetic isotope effect, and product studies, it is clear that the dominant pathway for the oxidation of formate is two-electron in character and involves the H–CO_2^- bond in an intimate way. The mechanism must involve a preassociation between the reactants, and, given the available experimental evidence, the preassociation step is followed by a redox step which must involve net hydride transfer.

$$[(bpy)_2(py)Ru^{IV}{=}O]^{2+} + HCO_2^- \overset{K_a'}{\rightleftharpoons} [(bpy)_2(py)Ru^{IV}{=}O]^{2+}, HCO_2^- \quad (4')$$

$$[(bpy)_2(py)Ru^{IV}{=}O]^{2+}, HCO_2^- \xrightarrow{k_{redox}} [(bpy)_2(py)Ru^{II}{-}OH]^+ + CO_2 \quad (6)$$

$$[(bpy)_2(py)Ru^{II}{-}OH]^+ + H^+ \xrightarrow[(rapid)]{} [(bpy)_2(py)Ru^{II}{-}OH_2]^{2+}$$

With this interpretation the experimentally measured rate constant, k_2, is, in fact, the product of the association constant, K_a', and the rate constant for the redox step, k_{redox}. Given the necessity of intimate interaction between the $Ru{=}O^{2+}$ and H–CO_2^- suggested by the large H/D kinetic isotope effect, K_a' is not simply the statistically derived association constant, K_a, given in eq 7. Equation 7 is valid assuming spherical reactants of radii r_A and r_B

$$K_a = \frac{4\pi N_o(r_A + r_B)^3}{3000} \exp(-w/RT) \quad (7)$$

N_o is Avogadro's number and w the electrostatic free energy change arising from formation of the association complex.[14] K_a' is the product of a K_a-like term and an orientational factor reflecting the fraction of association complexes in which the reactants have the appropriate relative orientation(s) for the redox step to occur.[14]

In earlier work based on metal-ion oxidants where there are displaceable ligands, e.g., Tl^{III}, Co^{III}, Mn^{III}, evidence is available to suggest the formation of intermediate formic acid or formato complexes.[15-17] Two characteristic features of these reactions are positive ΔS^* values (20–26 eu) and relatively small $k(H-CO_2^-)/k(D-CO_2^-)$ isotopic ratios (1.4–3.4). The Ru^{IV} complex is substitutionally inert at its normal coordination positions. Oxidation could occur via coordination expansion to give a seven-coordinate intermediate

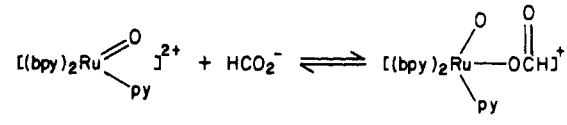

followed by an intramolecular redox step, however: (1) There is no evidence for the appearance of an intermediate early in the stopped-flow traces. (2) There is no precedence for coordination sphere expansion at Ru in this coordination environment. (3) The rate of $H_2{}^{18}O$ exchange with the bound oxo group, which could logically proceed via an intermediate like $[(bpy)_2(py)Ru^{IV}(OH)_2]^{2+}$, appears to be slow.[1,8]

Rather, it appears that mechanistically, $Ru^{IV}{=}O^{2+}$ should be grouped with the oxo-containing oxidants MnO_4^-[18] and Np^{VII}[19] whose reactions are characterized by large negative ΔS^* values (−14 and −31 eu, respectively) and sizeable H/D primary kinetic isotope effects (7 and 10, respectively). Comparative kinetics data for the oxidation of formate by MnO_4^-, Np^{VII}, or Ru^{IV}/Ru^{III} are collected in Table III.

Thermodynamics, Available Pathways. In Figure 6 are shown pH–potential plots for a series of couples of relevance to the oxidation of formate ion/formic acid by $Ru^{IV}{=}O^{2+}$. The data in Figure 6 were used to calculate free energy changes for the reactions in Scheme II. In Scheme II the reactions are grouped

(14) (a) Sutin, N. *Acc. Chem. Res.* **1982**, *15*, 275. (b) Sutin, N. *Prog. Inorg. Chem.* **1983**, *30*, 441.
(15) Halvorson, H. W.; Halpern, J. *J. Am. Chem. Soc.* **1956**, *78*, 5562.
(16) Varadarajan, R.; Wells, C. F. *J. Chem. Soc., Faraday Trans. 1* **1980**, *76*, 2017.
(17) Wells, C. F.; Whatley, D. *J. Chem. Soc., Faraday Trans. 1* **1972**, *68*, 434.
(18) (a) Taylor, S. M.; Halpern, J. *J. Am. Chem. Soc.* **1959**, *81*, 2933. (b) Taylor, S. M.; Halpern, J. *Discuss Faraday Soc.* **1965**, *29*, 174.
(19) Thompson, M.; Sullivan, J. C. *Inorg. Chem.* **1972**, *11*, 1707.

Table III. Comparative Kinetics Data for the Oxidation of Formate by Various Oxo Reagents

oxidant	substrate	$k^{25°C}$ (M^{-1} s^{-1})	$\Delta H^{\ddagger}$ (kcal/mol)	$\Delta S^{\ddagger}$ (eu)	k_H/k_D	ref
$(bpy)_2(py)Ru(O)^{2+}$	$HCOO^-$	4.3	7.7	−30	19	a
$(bpy)_2(py)Ru(OH)^{2+}$	$HCOO^-$	0.01			3	a
MnO_4^-	$HCOO^-$	3.0	12.4	−15	10	18a
MnO_4^-	$(NH_3)_5CoOCHO^{2+}$	0.21	13.3	−17	10.5	26
Np(VII)	$HCOO^-$	300			10	19

[a] This work.

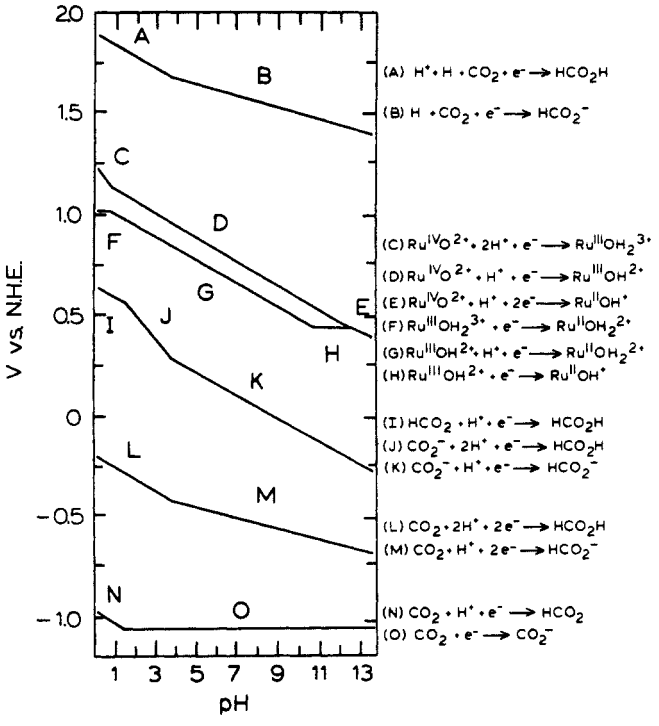

Figure 6. Potential pH diagrams for the ruthenium and formic acid couples of interest. Potentials for Ru couples from ref 1, $Ru^{IV}O^{2+}$ = $[(bpy)_2(py)Ru(O)]^{2+}$, $Ru^{III}OH^{2+}$ = $[(bpy)_2(py)Ru(OH)]^{2+}$, and $Ru^{II}OH_2^{2+}$ = $[(bpy)_2(py)Ru(OH_2)]^{2+}$. Potentials for formic acid couples from ref 18b and 30. The breaks in the plots coincide with an acid dissociation constant, e.g., $pK_a = 3.75$ for HCO_2H, and the slopes of the curves reflect the differences in proton and electron content for the couples as predicted by the Nernst equation: (1) $1e^-$; slope = 0 mV/pH unit, (2) $2e^-/1H^+$; 30 mV/pH unit, (3) $1e^-/1H^+$ or $2e^-/2H^+$; 59 mV/pH unit, (4) $1e^-/2H^+$; 118 mV/pH unit.

with regard to the number of e^- equiv involved in the elementary steps shown.

There are three reasonable mechanisms for the oxidation of HCO_2^- by $[(bpy)_2(py)Ru(O)]^{2+}$ given the large k_H/k_D kinetic isotope effect and Ru^{II} as the initial product. One is hydride transfer via eq 1.6 of Scheme II which is spontaneous by −43.1 kcal/mol. In the context used here, hydride transfer describes a process in which *synchronous* transfer of a proton and two electrons occurs from reductant to oxidant. Formation of a free hydride ion on a time scale long enough for the system to attain equilibrium with its surroundings is disfavored; $\Delta G = +92.0$ vs. kcal/mol from eq 1.8 in Scheme II.

The second and third possibilities both involve H-atom transfer in the initial step, in one case followed by rapid outer-sphere electron transfer (k_{et} in eq 8) before the initial redox products can separate from the surrounding solvent cage (k_{sep} in eq 8)

$$\begin{array}{ccc} (bpy)_2(py)Ru^{IV}{=}O^{2+},\ HCO_2^- & \longrightarrow & \\ (bpy)_2(py)Ru^{III}{-}OH^{2+},\ CO_2^- & \xrightarrow{k_{et}} & (bpy)_2(py)Ru^{II}{-}OH^{+},\ CO_2 \\ \downarrow k_{sep} & & \downarrow +H^+ \\ (bpy)_2(py)Ru^{III}{-}OH^{2+} + CO_2^- & & (bpy)_2(py)Ru^{II}{-}OH_2^{2+} + CO_2 \end{array} \quad (8)$$

In the other case, separation of $[(bpy)_2(py)Ru^{III}{-}OH]^{2+}$ and CO_2^- may occur but in order to explain $[(bpy)_2(py)Ru^{II}{-}OH_2]^{2+}$ as the initial Ru product, it is necessary to invoke selective oxidation of CO_2^- by Ru^{III}

$$(bpy)_2(py)Ru^{III}{-}OH^{2+} + CO_2^- \rightarrow (bpy)_2(py)Ru^{II}{-}OH^+ + CO_2$$

$$(bpy)_2(py)Ru^{II}{-}OH^+ + H^+ \xrightarrow[(rapid)]{} (bpy)_2(py)Ru^{II}{-}OH_2^{2+}$$

in competition with oxidation by Ru^{IV}

$$(bpy)_2(py)Ru^{IV}{=}O^{2+} + CO_2^- \rightarrow (bpy)_2(py)Ru^{III}{-}O^+ + CO_2$$

$$(bpy)_2(py)Ru^{III}{-}O^+ + H^+ \xrightarrow[(rapid)]{} (bpy)_2(py)Ru^{III}{-}OH^{2+}$$

Large k_H/k_D kinetic isotope effects have been found for H-atom transfer pathways involving $Ru^{IV}{=}O^{2+}$ [7,11] and rapid electron transfer between $[(bpy)_2(py)Ru^{III}{-}OH]^{2+}$ and CO_2^- is reasonable given the reaction

$$(NH_3)_5Ru^{III}(isn)^{3+} + CO_2^- \rightarrow (NH_3)_5Ru(isn)^{2+} + CO_2$$

where (isn is isonicotinamide) and k (23 °C, $\mu = 0.1$) = 1.04×10^{10} M^{-1} s^{-1}.[20] Oxidation of HCO_2^- by $Ru^{IV}{=}O^{2+}$ by H-atom transfer ($\Delta G = -15.2$ kcal/mol) is far less favorable than hydride transfer and although there is not direct experimental basis for choosing between H-atom and hydride transfer we favor the latter based on the following considerations: (1) There is good evidence in other studies that oxidation of C–H bonds by $Ru^{IV}{=}O^{2+}$ does occur by hydride transfer.[5,6] (2) The one-electron, relatively slow oxidation of HCO_2^- by $[(bpy)_2(py)Ru^{III}(OH)]^{2+}$ has a small k_H/k_D kinetic isotope effect (Table IV) and probably occurs by initial outer-sphere electron transfer

$$(bpy)_2(py)Ru^{III}{-}OH^{2+} + HCO_2^- \rightarrow (bpy)_2(py)Ru^{II}{-}OH^{2+} + HCO_2$$

followed by rapid proton equilibration to give $[(bpy)_2(py)Ru^{II}(OH_2)]^{2+}$ and CO_2^-.

In the oxidation of H_2O_2,[7]

$$(bpy)_2(py)Ru^{IV}{=}O^{2+} + H_2O_2 \rightarrow (bpy)_2(py)Ru^{III}{-}OH^{2+} + HO_2$$

both $Ru^{IV}{=}O^{2+}$ and $Ru^{III}{-}OH^{2+}$ utilize H-atom pathways, and the two are comparable ratewise with the enhanced rate for $Ru^{IV}{=}O^{2+}$ attributable to the ~100 mV greater potential for the $Ru^{IV}{=}O^{2+}/Ru^{III}{-}OH^{2+}$ couple compared to the $Ru^{III}{-}OH^{2+}/Ru^{II}{-}OH_2^{2+}$ couple. The inability of $[(bpy)_2(py)Ru^{III}(OH)]^{2+}$ to find a competitive, relatively facile H-atom pathway in the oxidation of HCO_2^- suggests that a facile H-atom pathway may not exist for $[(bpy)_2(py)Ru^{IV}(O)]^{2+}$ which is competitive with hydride transfer.

Magnetic studies on $[(bpy)_2(py)Ru(O)]^{2+}$ show that the complex is a ground-state singlet but with a low-lying magnetic triplet state.[1b] The magnetism is consistent with a pattern of lowest levels consisting of a degenerate or nearly degenerate set of $d\pi$ levels which would be largely d_{xz} and d_{yz} in an axis system where the Z axis lies along the Ru=O bond. From the results of the magnetic study and IR evidence for multiple Ru–O bonding (ν(Ru=O) = 792 cm^{-1}), the acceptor orbitals for the $Ru{=}O^{2+}$ oxidant are a pair of largely metal based d_{xz}, d_{yz} orbitals but with considerable $p_x(O)$ and $p_y(O)$ character arising from $d\pi(Ru)$–$p(O)$ mixing with the oxo group.

(20) Stanbury, D. M.; Mulac, W. A.; Sullivan, J. C.; Taube, H. *Inorg. Chem.* **1980**, *19*, 3735.

Given the electronic properties of the oxidant and the evidence for hydride transfer, it is possible to reach some reasonable conclusions concerning the nature of the electronic interactions which provide a basis for the redox step. They include the following: (1) Weak initial outer-sphere electronic coupling between the reactants—$Ru^{IV}{=}O^{2+}$, HCO_2^-—and initial redox products—Ru^{II}—OH^+, CO_2. (2) Strong $\nu(H-CO_2^-)$ induced electronic coupling between $\sigma(C-H)$ and the $d_{xz} + p_x(O)$ or $d_{yz} + p_y(O)$ acceptor orbitals. A contributing factor to the enhanced rate of oxidation of HCO_2^- compared to HCO_2H may be the higher relative energy of $\sigma(C-H)$ for HCO_2^-[21] which would enhance the degree of electronic interaction between $\sigma(C-H)$ and the $d\pi$ acceptor orbitals of the oxidant. (3) As electron flow into the acceptor orbital becomes significant, an O-localized electron pair on the oxo ligand becomes available for donation to the transferring proton. (4) The concerted nature of the process is assured by the highly unfavorable energetics associated with formation of a free hydride ion in a step like, $Ru^{IV}{=}O^{2+}$, $H-CO_2^- \rightarrow [Ru^{IV}O^{2+}, H^-, CO_2]$, eq 1.8 in Scheme II. (5) Since $Ru^{IV}{=}O^{2+}$ is a ground-state magnetic singlet, there is a net spin change in the hydride transfer step, $^1[(bpy)_2(py)Ru^{IV}(O)]^{2+}$, $HCO_2^- \rightarrow {}^1[(bpy)_2(py)Ru^{II}(OH)]^+$, CO_2 and no basis for spin restrictions.

Of the three types of available pathways for the oxidation of formate ion by the substitutionally inert $Ru^{IV}{=}O^{2+}$ complex—outer-sphere electron transfer, H-atom transfer, and hydride transfer—outer-sphere electron transfer is the most simple and primitive mechanistically. Its reaction demands include association between reactants, weak electronic orbital overlap, and thermally activated electron transfer. Outer-sphere electron transfer is not a competitive pathway in the oxidation of formate ion by $Ru^{IV}{=}O^{2+}$ in part because of the relatively unfavorable energetics of forming deprotonated Ru^{III} as $[(bpy)_2(py)Ru^{III}(O)]^+$ and the unstable one-electron intermediate and HCO_2 (eq 1.4 in Scheme II). In the classical limit the dependence of the outer-sphere electron transfer rate constant, k_{et}, on ΔG is predicted to be of the form $k_{et} \propto \exp-[(\lambda + \Delta G)^2/4\lambda RT]$ where λ is the sum of the intramolecular and solvent trapping barriers to electron transfer. The appearance of high energy intermediates increases ΔG and decreases k_{et}.

In comparing mechanistic demands for H-atom

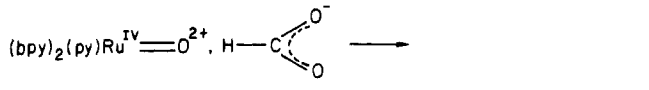

and hydride transfer

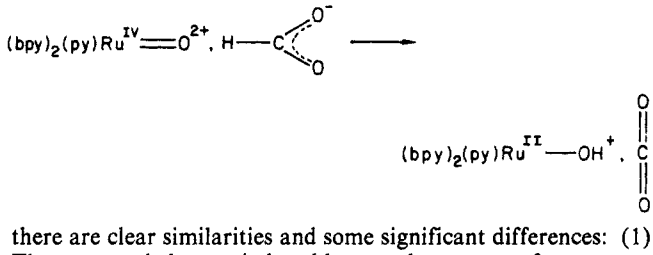

there are clear similarities and some significant differences: (1) The structural changes induced by two-electron transfer are more profound both at HCO_2^-, where linear CO_2 rather than bent CO_2^- is the initial product, and at $Ru^{IV}{=}O^{2+}$, where a greater Ru–O bond length change is expected for Ru(IV) → (II) compared to Ru(IV) → (III). (2) There are no spin restrictions to either reaction. (3) As for electron transfer, hydride transfer involves the net transfer of charge between reactants and products, and an additional activational contribution must exist arising from the reorientation of solvent dipoles when the reactants are converted into products.[22]

(21) Maria, H. J.; Larson, D.; McCarville, M. E.; McGlynn, S. P. *Acc. Chem. Res.* **1970**, *3*, 368.

(22) Endicott, J. F.; Kumar, K.; Ramasami, T.; Rotzinger, F. P. *Prog. Inorg. Chem.* **1983**, *30*, 141.

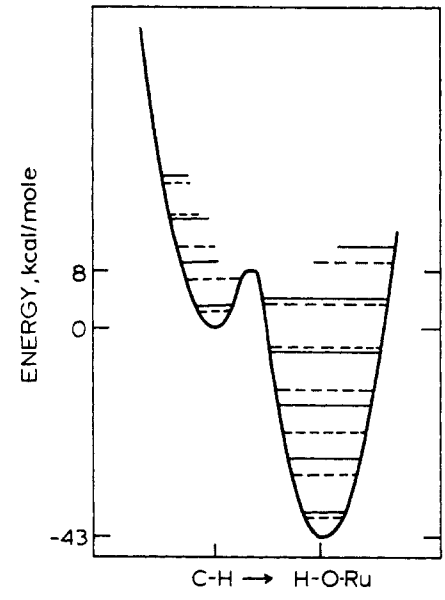

Figure 7. Potential curves for the $\nu(H-CO_2^-)$ and $\nu(H-ORu)$ normal modes and their intersection illustrating schematically the potential curve for the hydride transfer: $(bpy)_2(py)Ru^{IV}{=}O^{2+}$, $HCO_2^- \rightarrow (bpy)_2(py)Ru^{II}$—$OH^{2+}$, CO_2. The vibrational spacings are 2830 cm^{-1} for $\nu(H-C)$ and 3455 cm^{-1} for $\nu(H-O)$ with the $\nu(D-C)$ and $\nu(D-O)$ levels shown as dashed lines. The force constants used to construct the curves were $k(H-C)$ = 487 mdyn/cm and $k(H-O)$ = 599 mdyn/cm.[23]

Even though the activational requirements favor H-atom over hydride transfer, hydride transfer may be the pathway of choice because of the considerable energy advantage enjoyed by a two-electron step which avoids the high energy, one-electron intermediate, CO_2^- (eq 1.2 and 1.6 in Scheme II).

Kinetic Isotope Effects. Given the nature of the hydride transfer pathway, contributions to the interconversion between reactants and products are expected from vibrational modes like $\nu(Ru{=}O)$ at the Ru^{IV} oxidant and $\delta(OC)$ bending at formate. However, from the considerable magnitude of the H/D kinetic isotope effect, it seems clear that the dominant vibrational contributors to the reaction are normal modes having appreciable $\nu(H-CO_2^-)$ character in the formate reactant and $\nu(H-ORu)$ character in the Ru^{III} product.

In Figure 7 are shown the following: (1) Harmonic oscillator potential curves for the $\nu(H-CO_2^-)$ and $\nu(H-ORu)$ modes using $\nu(H-C)$ = 2830 and $\nu(H-O)$ = 3455 cm^{-1} and the force constants $k(H-C)$ = 487 mdyne/cm and $k(H-O)$ = 599 mdyne/cm.[23] (2) The various energy quantities appropriate for hydride transfer are also illustrated including the internal energy change for the redox step (ΔG = −43 kcal/mol), the vibrational spacings for $\nu(D-CO_2^-)$ and $\nu(D-ORu)$ (dashed lines), and the experimentally observed energy of activation for oxidation of HCO_2^- (E_a = 7.9 ± 0.9 kcal/mol). On this scale the approximate energy required if the reaction proceeded via a discrete hydride ion intermediate in the step, $Ru^{IV}{=}O^{2+}$, $HCO_2^- \rightarrow Ru^{IV}{=}O^{2+}$, H^-, CO_2 would appear at +92 kcal/mol. (3) The curve connecting the two harmonic oscillators is a two-dimensional, schematic attempt to illustrate a linear combination of the $Q(H-CO_2^-)$ and Q(H–ORu) coordinates which lead to electronic coupling between $Ru^{IV}{=}O^{2+}$ and HCO_2^- and to the interconversion between reactants and products.

The experimental facts pertaining to the H/D kinetic isotope effect show that it is not amenable to simple interpretation. The effect is large and considerably temperature dependent; k_H/k_D varies from 22 at 289.6 K to 16 at 311.4 K. From the temperature dependent data taken near room temperature (289.6–311.4 K), the difference in the energies of activation is $E_a(DCO_2^-) - E_a(HCO_2^-)$ = 3.2 kcal/mol, and the ratio of preexponential factors is 7.

(23) Gregory, A. R.; Kidd, K. G. *J. Mol. Spectrosc.* **1981**, *85*, 375.

The temperature dependence of k_H/k_D has been treated for simple outer-sphere electron-transfer reactions where electronic coupling between reactants is weak.[24,25] In treatments of this kind electron transfer occurs as a nonradiative transition from the vibrational levels of the initial (reactants) to final (products) potential curves. Transition rates are higher for levels near the intersection region between potential curves because overlap of vibrational wave functions between the initial and final states is higher. Maximum k_H/k_D isotope effects are predicted to occur at very low temperatures where transitions are dominated by levels close to $v = 0$, and in the parlance of the solid state physics literature, the reaction occurs by "nuclear tunneling". At $v = 0$, the lower zero-point energy ($^1/_2h\nu$) for the deuterium-substituted case ensures that the vibrational overlap differences between the ν(A–H) and ν(A–D) modes are maximized. A larger E_a is expected for the deuterium case because of the importance of thermal population of levels nearer the intersection region where vibrational overlaps are higher. The energy of activation is predicted to be temperature dependent for either case until low temperatures where the reactions are dominated by transitions from $v = 0$ levels.

Some attempts have been made to treat H-atom transfer quantitatively in order to account, for example, for data obtained for H-atom abstraction from CH_3OH or CH_3CN in low-temperature glasses.[26] In such treatments electronic coupling is included in the form of a potential curve for the transferring H-atom, and vibrational overlap or tunneling calculations are made to calculate transition rates.

Comparisons with Other Systems. In an earlier section note was taken of the fact that for oxidants like Tl^{III}, Mn^{III}, or Co^{III}, formate oxidation occurs by prior coordination. However, clear similarities appear to exist between the pathways for oxidation of HCO_2^- by $Ru{=}O^{2+}$, MnO_4^-, or Np^{VII} as shown by the collected data in Table III. Data pertaining to the oxidation of formate bound to Co^{III} are also included.[27] From the data in Table V the reactions involving oxo reagents have relatively large k_H/k_D kinetic isotope effects. However, there is a distinct difference in the pattern of activation parameters, and the mechanisms may be different.

As shown by comparing the MnO_4^- oxidation of HCO_2^- and of $[(NH_3)_5CoO_2CH]^{2+}$, the larger $\Delta H^{\ddagger}$ and $\Delta S^{\ddagger}$ values for MnO_4^- compared to $Ru^{IV}{=}O^{2+}$ cannot be attributed entirely to electrostatic effects on the preassociation constant, K_a'. In fact, there is evidence that the MnO_4^- oxidations occur via an initial one-electron step as evidenced by the appearance of Co^{II} as a product, apparently via,[27]

$$(NH_3)_5Co^{III}O_2CH^{2+} + MnO_4^- \rightarrow (NH_3)_5Co^{III}O_2C^{2+} + HOMnO_3^-$$

$$(NH_3)_5Co^{III}O_2C^{2+} \xrightarrow{+5H^+} Co(II) + 5NH_4^+ + CO_2$$

Of additional interest is the result of an ^{18}O labeling study on the oxidation of HCO_2^- by MnO_4^- by Wiberg and Stewart.[28] They found that ca. 30% of the label from ^{18}O labeled permanganate appeared in the CO_2 product after formate oxidation. Reconciling their observation with the large H/D kinetic isotope effect and the apparent one-electron nature of the initial redox step is difficult. However, one possibility is that incorporation of the label arises *after* the rate-determining step through the capture of CO_2^- by MnO_4^-

$$H^+ + O_3Mn^{VII}O^- + CO_2^- \rightarrow O_3Mn^{VI}OCO_2H^- \quad (9)$$

Scrambling of the carbonate oxygens and subsequent loss of CO_2 would account for the observation of ^{18}O in the CO_2 product.[29] Taube has proposed a similar intermediate in the oxidation of $[(NH_3)_5CoOCHO]^{2+}$ by MnO_4^-.[30]

Reduction of CO_2. The results obtained here bear directly on the existence of possible pathways for the microscopic reverse of formate oxidation, reduction of CO_2 to formate. Particularly notable in this regard is the appearance of the hydride transfer pathway

$$[(bpy)_2(py)Ru^{IV}{=}O]^{2+}, HCO_2^- \rightarrow [(bpy)_2(py)Ru^{II}{-}OH]^+, CO_2$$

The appearance of oxidative hydride transfer suggests the possibility of utilizing low-oxidation state aquo or hydroxo couples as catalysts for the microscopically reverse reaction, reduction of CO_2 to HCO_2^- via

$$M{-}OH^{n+}, CO_2 \rightarrow M{=}O^{(n+1)+}, HCO_2^-$$

In this regard it is disappointing that the oxidative step, which is thermodynamically favored by ~43 kcal/mol, is so slow. Even if the reverse pathway exists, the kinetic demands imposed by the reduction may be so severe that rates will be too slow to be of value catalytically.

Acknowledgments are made to the Gas Research Institute under Grant No. 5083-260-0827 and to the National Science Foundation under Grant No. CHE-8304230 for support of this research.

Registry No. $HCOO^-$, 71-47-6; $[(bpy)_2(py)Ru(O)](ClO_4)_2$, 67202-44-2; $[(bpy)_2(py)Ru(OH)]^{2+}$, 75495-07-7; HCOOH, 64-18-6; D_2, 7782-39-0.

Supplementary Material Available: A table of rate constants for the temperature dependence of the oxidation of HCO_2^- and DCO_2^- by $[(bpy)_2(py)Ru(O)]^{2+}$ at $\mu = 1.0$ M (Na_2SO_4) at pH 7 (2 pages). Ordering information is given on any current masthead page.

(24) Buhks, E.; Bixon, M.; Jortner, J. *J. Phys. Chem.* **1981**, *85*, 3763.
(25) Guarr, T.; Buhks, E.; McLendon, G. *J. Am. Chem. Soc.* **1983**, *105*, 3763.
(26) LeRoy, R. J.; Muria, H.; Williams, F. *J. Am. Chem. Soc.* **1980**, *102*, 2325.
(27) Candlin, J. P.; Halpern, J. *J. Am. Chem. Soc.* **1963**, *85*, 2518.
(28) Wiberg, K. B.; Stewart, R. *J. Am. Chem. Soc.* **1956**, *78*, 1214.
(29) Stewart, R. In *Oxidation in Organic Chemistry, Part A*; Wiberg, K., Ed.; Academic Press: New York, 1965; Chapter I.
(30) Taube, H. *Electron Transfer Reactions of Complex Ions in Solution*; Academic Press: New York, 1970; Chapter IV.
(31) Endicott, J. F. In *Concepts of Inorganic Photochemistry*; Adamson, A. W., Fleischauer, P. D., Eds; Wiley: New York, 1975; Chapter 3.